

Objective Lenses for Confocal Microscopy

H. Ernst Keller

INTRODUCTION

No other component of the microscope is as instrumental in determining the information content of an image as the objective. The resolved detail, the contrast at which this detail is presented, the depth through the object from which useful information can be derived, and the diameter of the useful field are all limited by the performance of the objective. All other imaging components, such as relay optics, Telan systems, tube lenses and eyepieces, or projectives may have some corrective function but otherwise serve only to present the image generated by the objective to the detector in such a way that most of its information content can be recorded without degradation.

While this is true for any conventional microscope, it is particularly true for confocal scanning, where the objective becomes the condenser as well and needs to combine a high degree of optical correction with good throughput and a minimum of internal stray light or photon noise generation.

In general, the demands on the performance of the objective for confocal scanning are identical to the needs for demanding video microscopy, photomicroscopy, densitometry, photometry, spectrophotometry, and morphometry. However, this does not mean that confocal microscopy will not eventually call for special new lenses in which certain corrections may be sacrificed to enhance specific capabilities. In biological applications involving living cells, high photon efficiency is so important that it may be worth accepting a reduction in field size and chromatic correction in order to achieve the highest possible transmittance at a reasonable working distance by using a minimum number of lens elements. Another problem is the loss of correction for spherical aberration as an oil-immersion lens is focused deep into an aqueous specimen. High numerical aperture (NA) water-immersion objectives with correction collars for coverslip thickness variations, refractive index variations in the medium, or temperature-dependent index changes have become the lenses of choice for live-cell studies. Because of the difficulty manually rotating the correction collar while actually observing living specimens, correcting spherical aberration may require the addition of either deformable mirror correctors or motor-driven correction optics mounted later in the optical path (see also Chapter 20, *this volume*).

Because the critical demands of light microscopy and confocal scanning microscopy have increasingly forced the performance of objectives to approach their theoretical limits, a brief refresher on aberrations, design concepts, materials, etc., may be in order. An overview of optical aberrations in refractive systems — both

inherent and induced by improper use of the microscope — and the basic performance characteristics of the different generic types of objectives will be presented.

The basic design concepts of microscope optics — finite versus infinite image distance, compensating versus fully corrected systems — need to be understood to properly match optical components and their properties for specific applications. Optical materials, cements, and anti-reflection coatings all influence the performance of the objective. Immersion liquids, the coverslip, and the mounting medium are all part of the optical train and can strongly affect the quality of the final image. We will try to put all of this into qualitative perspective, particularly as it pertains to confocal scanning. Additional information on the optics for microscopy can be found in a review paper by Inoué and Oldenbourg (1995) and in a review article on objective lens design by Shimizu and Takenaka (1994).

A detailed, quantitative comparison of the performance of different microscope objectives must be based on accepted criteria and precisely defined testing methods. Unfortunately, although the major microscope makers have developed their own proprietary methods, no independent, fully “objective” test procedure is readily accessible to users to quantify all performance data of an objective. (Juskaitis describes a sophisticated means for interferometric testing of objectives in Chapter 11, *this volume*.)

How, then, should the user of a confocal microscope judge the performance of an objective? Measurement and analysis of the real, not just theoretical, point spread function (PSF) of an objective, or better, of the complete imaging system, is critical for three-dimensional (3D) deconvolution. Observations of subresolution pinholes in an evaporated silver or aluminum coating are adequate to judge spherical aberration, astigmatism, coma, and flatness in transmitted light but do not work well in the epi-mode. Fluorescent beads in the 0.1 μm range are suitable replacements, but the fluorescence fades. Diatoms have long been a standard because of their precise and regular spacing and because they can be viewed in the backscattered (BSL, sometimes referred to as reflected) light mode or after embedment in fluorescent dye (Chapter 35, *this volume*). For example, how do we determine, at least qualitatively, how an image is degraded — by focusing deep into a specimen or by pairing optical components that are not matched? These are all challenges that are not yet fully resolved. They point to a need for detailed testing procedures that cover all aspects of the optics from source to detector.

Still, with our ability today to ray-trace lenses for their geometrical optical performance and to calculate wave-front aberrations, PSF, and intensity ratios through the Airy disk, most

objectives now offered are close to diffraction limited, at least in the center of the image field. However, field size and optical performance at the periphery of the field are also especially important in beam-scanning confocal microscopy.

Long-term mechanical, thermal, and chemical stability of objectives used with lasers are a function of manufacturing tolerances and materials chosen. Submicron tolerances for the centration and spacing of lens elements in sophisticated, high-power objectives call for careful, gentle treatment by the user. A minor mechanical shock may generate enough stress on a lens element to seriously reduce the objective's performance in polarized light, in differential interference contrast (DIC), or in critical confocal scanning.

ABERRATIONS OF REFRACTIVE SYSTEMS

The ideal “diffraction-limited” objective generates a 3D PSF from an infinitely small object point. A cross-section perpendicular to the optical axis through the center of the PSF is the Airy disk, as shown in Figure 7.1(A). The diameter d_{Airy} of the first dark ring, generated by destructively interfering, diffracted wavefronts [Fig. 7.1(B)] is

$$d_{\text{Airy}} = \frac{1.22\lambda}{\eta \sin\alpha}$$

where λ is the wavelength of light, η is the refractive index of medium between the object and the objective, and α is the half-angle of the collected rays from the object point. The Rayleigh (or Abbe) criterion sets the limit for the smallest resolvable distance d between two points at one-half this diameter or,

$$r_{\text{Airy}} = \frac{1.22\lambda}{2 \text{NA}}$$

or the radius of the Airy disk, where $\eta \sin\alpha$ is the NA. This point-to-point resolution for a given objective in turn determines the magnification required to enable any given detector to record all the resolvable details. Taking the spacing of the rods in the human retina as setting the limit, the total required magnification for visual observation — the so-called useful magnification — becomes about 500 to 1000 times the NA of the objective, while for digital recording we enlarge the Airy disk to 4 to 5 times the pixel dimension of the detector (Nyquist sampling, see Chapter 4, *this volume*).

Defocusing

Defocusing will change the size and intensity distribution of the unit image point (Fig. 7.2). Because defocusing and depth of field are closely related, let us take a look at the 3D PSF or “image body” of the “diffraction limited” objective (Chapter 1, *this volume*).

Figure 7.3 again shows a cross-section perpendicular to the optical axis in the optimally focused image/object plane, which is, of course, the intensity distribution of the Airy disk, while Figure 7.4 represents a section along the optical axis and its intensity distribution (actually, the log of the intensity, to make it more visible). Defocusing results in alternating bright and dark spots along the axis of the Airy disk (Fig. 7.2). The extension of the central bright body along the axis is $4\lambda/(\text{NA})^2$, but we can detect a change in the image with a defocus of only $\pm\lambda/(\text{NA})^2$ (the Rayleigh/Abbe unit in the z -direction). We call this the wave-optical depth of field (Figs. 7.3 and 7.4).

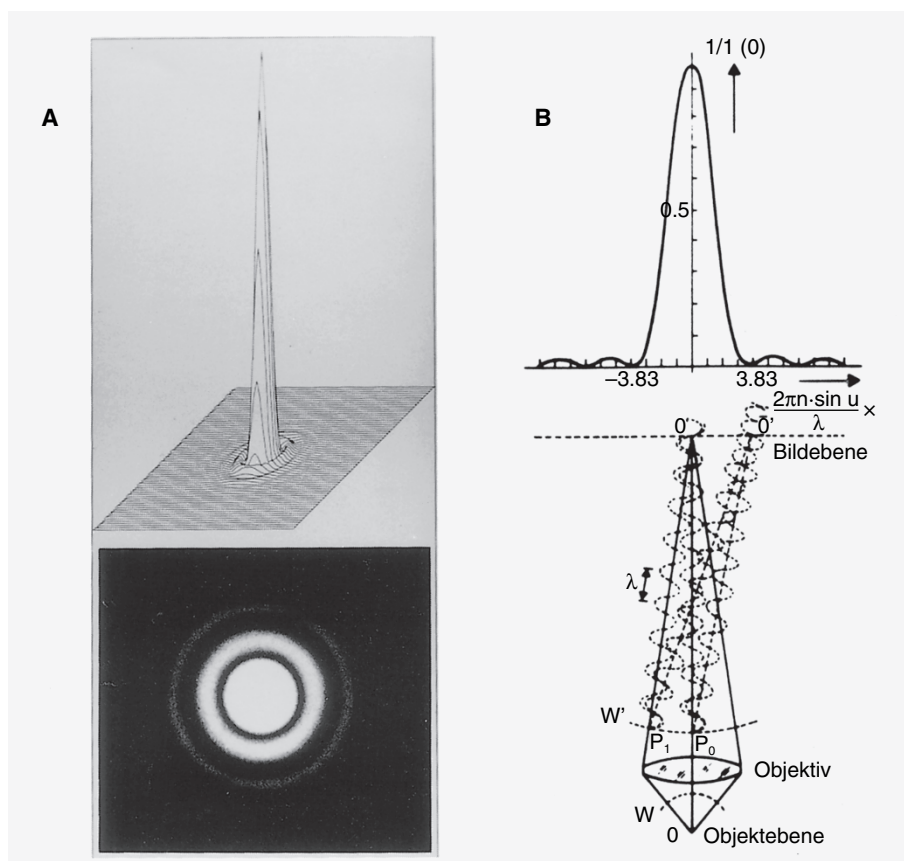


FIGURE 7.1. (A) Airy disk and its intensity distribution. (B) Generation diagram and profile of the Airy disk or unit image.

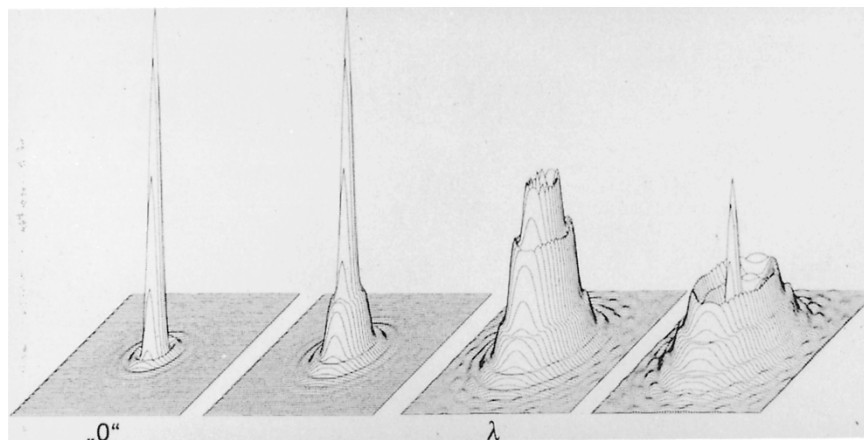


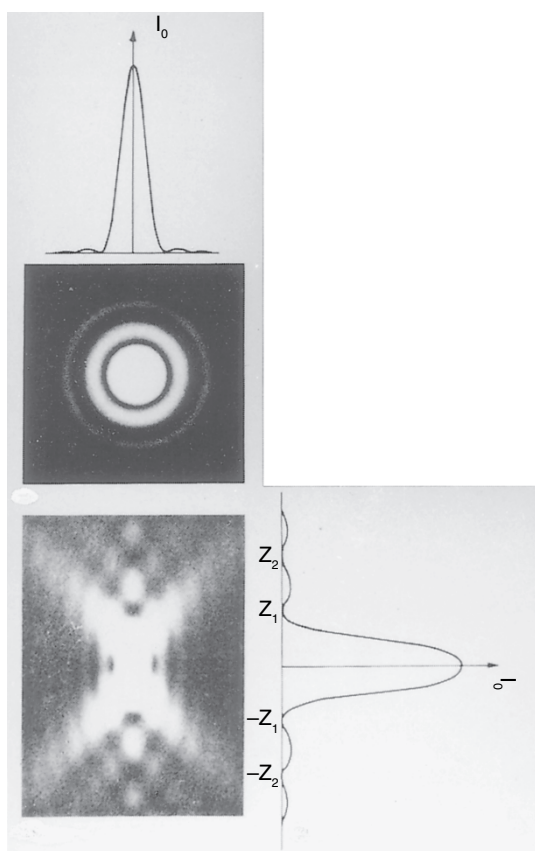
FIGURE 7.2. Changes in intensity distribution with focus changes.

Deviations from the “diffraction-limited” point image caused by lens aberrations can be grouped into either wavelength-independent (monochromatic) or chromatic aberrations.

Monochromatic Aberrations

Spherical Aberration

This axial aberration is generated by non-spherical wavefronts produced by the objective itself or by improper use of the objective,



FIGURES 7.3 and 7.4. Horizontal (focal plane) and vertical (optical axis) cross-section through unit image body.

in particular, failure to use the correct coverglass thickness or maintain the designated tube length or the presence of substances between the objective and the focus plane having the wrong n (Chapter 20, *this volume*). Spherical aberration has the effect that paraxial rays have a different focal length from peripheral rays, and a blurring of the image body produces an asymmetrical intensity change when defocusing by $\pm\Delta Z$ (Fig. 7.5 and Fig. 20.3, *this volume*). Spherically ground and polished lenses have a shorter focal distance for peripheral rays than for paraxial rays.

Spherical aberration can be optimally corrected only for accurately specified object and image distances. It can, therefore, be easily induced by improper tube length caused by introduction of optical elements into the converging beam path of finitely designed systems or by the use of improper “windows,” such as non-standard coverslips or immersion oil of non-specified refractive index between object and objective. Figure 7.6 shows the changes in size and intensity distribution through the image point with increasing penetration into an object in watery medium with a planapochromat 63 \times , NA 1.4 oil. The effect of this induced spherical aberration on the image point needs to be considered and either corrected for or at least understood before confocal microscopy can be applied optimally to 3D reconstruction (see Chapter 24, *this volume*). More specifically, let us consider how the image quality of another objective designed for diffraction-limited performance (the Plan-Neofluar 40 \times , NA 1.3 oil) deteriorates when focusing 10 μm into an aqueous medium.

At the water–coverslip interface, spherical aberration is generated, which shifts the focus of peripheral rays above the optimal focus of paraxial rays [Fig. 7.7(A,B)].

Figure 7.8 illustrates the change in intensity of a fluorescing object detected with a pinhole equal to the diameter of the Airy disk (1 Airy Unit) at 543 nm as a function of different penetration depths or focus changes, indicated in both micrometers and Rayleigh units (RE) into water. For depths of 0 μm , 5 μm , 10 μm , and 20 μm , the signal intensity at the pinhole detector drops dramatically along with deteriorating depth discrimination. Minor changes in refractive index are generated by changes in salt concentration, temperature, and differences in molecular structure. All these can induce positive or negative spherical aberration.

With increasing NA, changes in the thickness or the refractive index of the “window” between the object and the objective becomes critical, particularly with “dry” objectives. In the low-power, low-NA objective with relatively higher $NA_{\text{imageside}}$ where

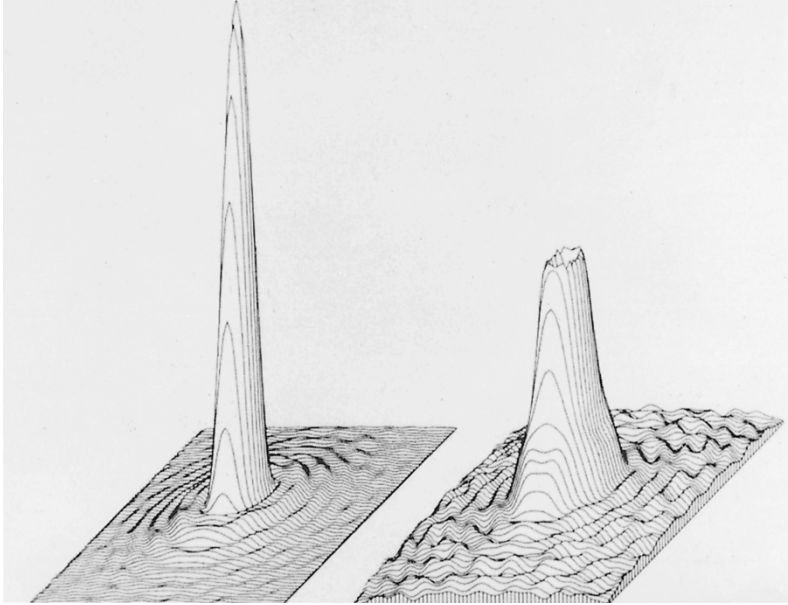


FIGURE 7.5. Nonsymmetrical change in the intensity distribution with focus change above (left) and below (right) best focus in a system limited by spherical aberration.

$$NA_{\text{imageside}} = \frac{NA_{\text{objectside}}}{\text{Magnification}}$$

small changes in tube length quickly lead to inferior images.

While the spherical aberration can be corrected to less-than-perceptible limits for visual observation for all types of objectives, this holds true only if all optical specifications for a given lens are fulfilled. For oil-immersion lenses with high NA, this usually means using a coverslip of 0.17 mm thickness, and $\eta = 1.518$ at 546 nm and 589 nm and an immersion oil with $\eta = 1.5180 \pm 0.0004$ at 546 nm or $\eta = 1.515$ at 589 nm, a condition complicated by the fact that, in all materials, η is a function of λ and temperature. If the exact properties of the coverslip and the oil are specified, then the manufacturer can correct spherical aberration for several values of λ : Zeiss achromats are corrected for 2λ s, neofluars for 3λ s, and planapochromats for 4λ s.

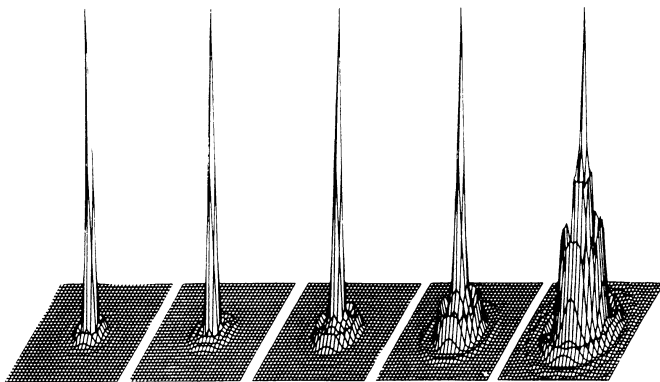


FIGURE 7.6. Change in the intensity distribution with increasing penetration into a watery medium with a planapochromat. Penetration depth from 0 to $4\mu\text{m}$. Note: In these plots, peak intensity has been normalized. In practice, it should decrease dramatically as the base of the intensity plot widens.

With high NA dry or water-immersion objectives, the thickness of the coverslip, standardized throughout the industry as 0.17 mm (# 1.5), is particularly important. Figure 7.9 shows the changes in the half-width of the intensity distribution curve with changes in coverslip thickness. With tolerances of $\pm 10\mu\text{m}$ for top-quality coverslips, the half-width can change by more than a factor of 2. With increasing NA (>0.5), particularly with dry and water-immersion lenses, selection of coverslips for correct thickness is particularly important. Even oil-immersion lenses such as the planapochromat

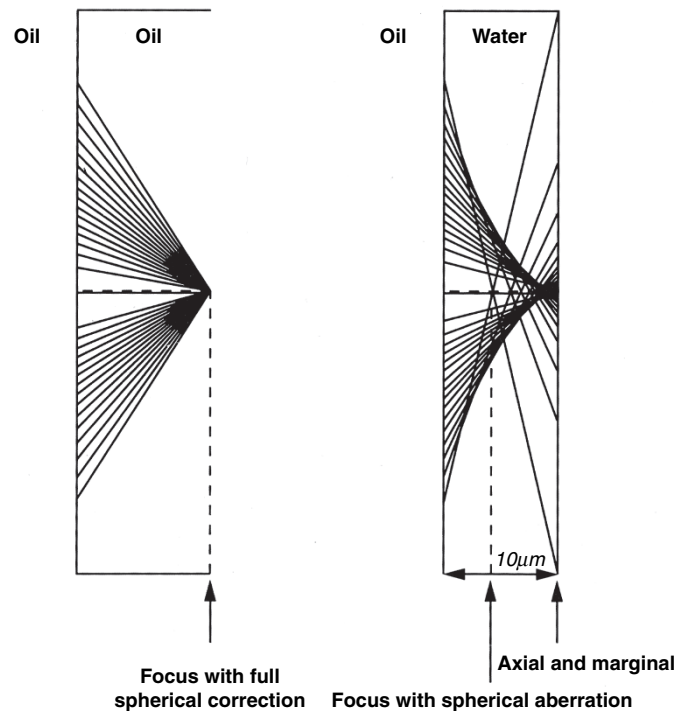


FIGURE 7.7. Ray diagram of an NA = 1.3 oil-immersion objective, focusing into oil (left) versus focus $10\mu\text{m}$ in water (right).

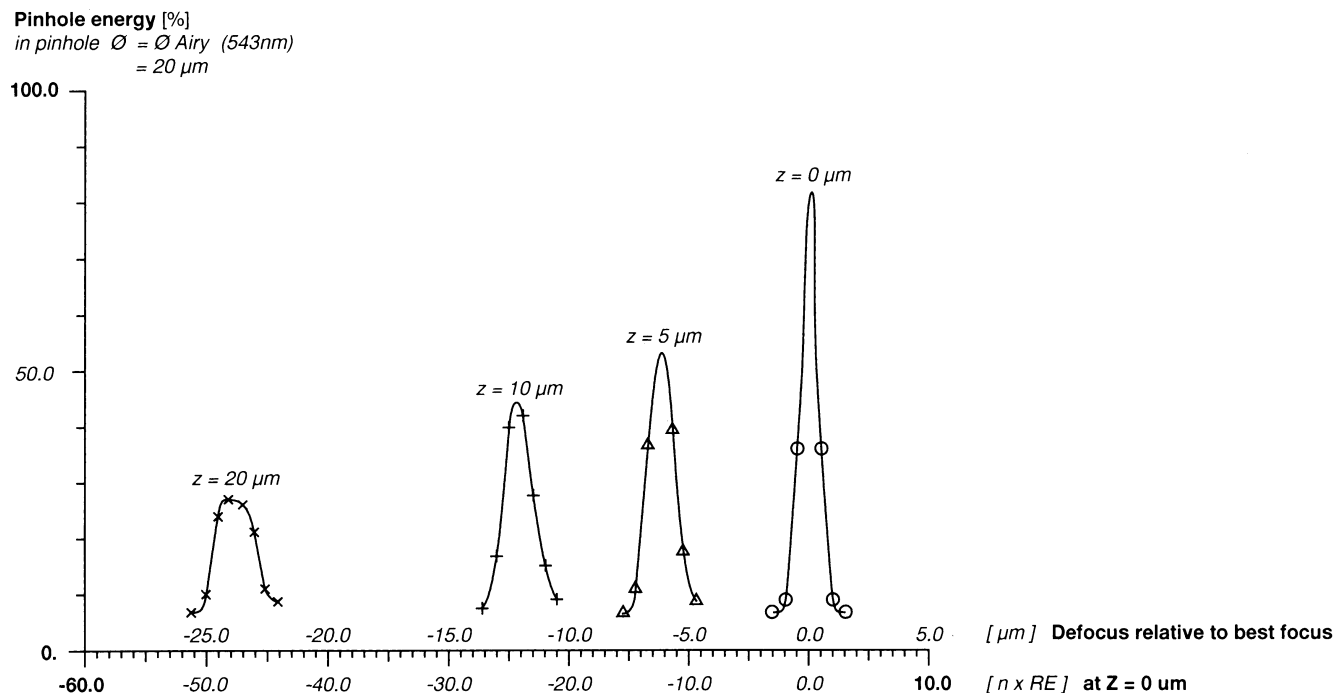


FIGURE 7.8. Pinhole energy measured through a 40 \times , NA 1.3 oil objective; as function of defocus and depth of penetration (Z) into water. As the thickness of the water layer increases from 0 and 50 μm , the resolution is reduced by about 3 \times and the intensity by a similar amount.

63 \times , NA 1.4 perform optimally only with a coverslip thickness of 0.17 mm (Chapter 8, *this volume*). Fortunately, electro-mechanical micrometers capable of reading coverslip thickness to an accuracy of $\pm 1 \mu\text{m}$ are now available at relatively low cost.

The spherical aberration induced by non-specified coverslip thickness leads to loss of energy at the pinhole, reduced depth discrimination, and an axial shift of the best focus. This is shown in Figure 7.10 for a diffraction-limited, water-immersion 40 \times , NA 1.2 objective.

These examples underline the importance of maintaining the specified and computed optimal conditions for microscope objectives in order to achieve the full benefits of confocal microscopy.

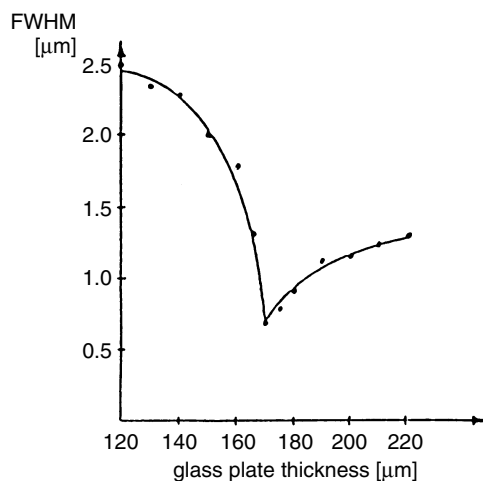


FIGURE 7.9. Changes in the half-width of the intensity distribution with changing coverslip thickness. Plan-Neofluar 63 \times , NA 1.2 water.

On high-NA, dry objectives or on multi-immersion objectives, eliminating induced spherical aberration requires that the correction collar be set exactly ($\pm 2 \mu\text{m}$ of glass-replaced-by-water at NA 1.2, see Figs. 7.9 and 20.3).

From the above, it becomes obvious that a water-immersion objective is the best choice to minimize induced spherical aberration when penetrating aqueous media. Unfortunately, the collection of 3D data requires moving the specimen with respect to the lens. If this is not to produce motion of the specimen, a coverslip must be used. Experiments have shown, however, that precise correction for coverslip thickness or even the use of “Cytos” (a new coverslip material with a refractive index of 1.34, which is almost that of water, developed by Olympus) will not suffice. The refractive differences in physiological media and in biological materials still require systems that permit adjustable correction for the spherical aberration induced by the specimen itself (see Figs. 2.3–2.5, *this volume*).

With the introduction of high-NA water-immersion objectives designed for coverglass use, some with working distances of 0.24 mm, microscopy on live cells or tissue has been greatly facilitated. Their correction collars not only allow one to compensate for variations in the coverglass thickness (after it has been measured with a micrometer or via the confocal software) but also allows one to compensate for refractive index changes due to temperature or concentration changes in the medium. Although these water-immersion objectives have nominally lower NAs than comparable oil lenses, keep in mind that the effective NA of the oil objective, when looking through water, is dictated by the refractive index of the water or of the medium of lowest refractive index between object and objective. For most aqueous specimens the water-immersion lens is clearly the preferred choice.

Not all experiments permit optimal imaging conditions, and the question arises whether objectives with lower NA or with a built-in iris would not sometimes yield better results. Figure 7.11 again plots

Pinhole energy
 in pinhole $\emptyset = \emptyset$ Airy (543nm)
 = 23 μm

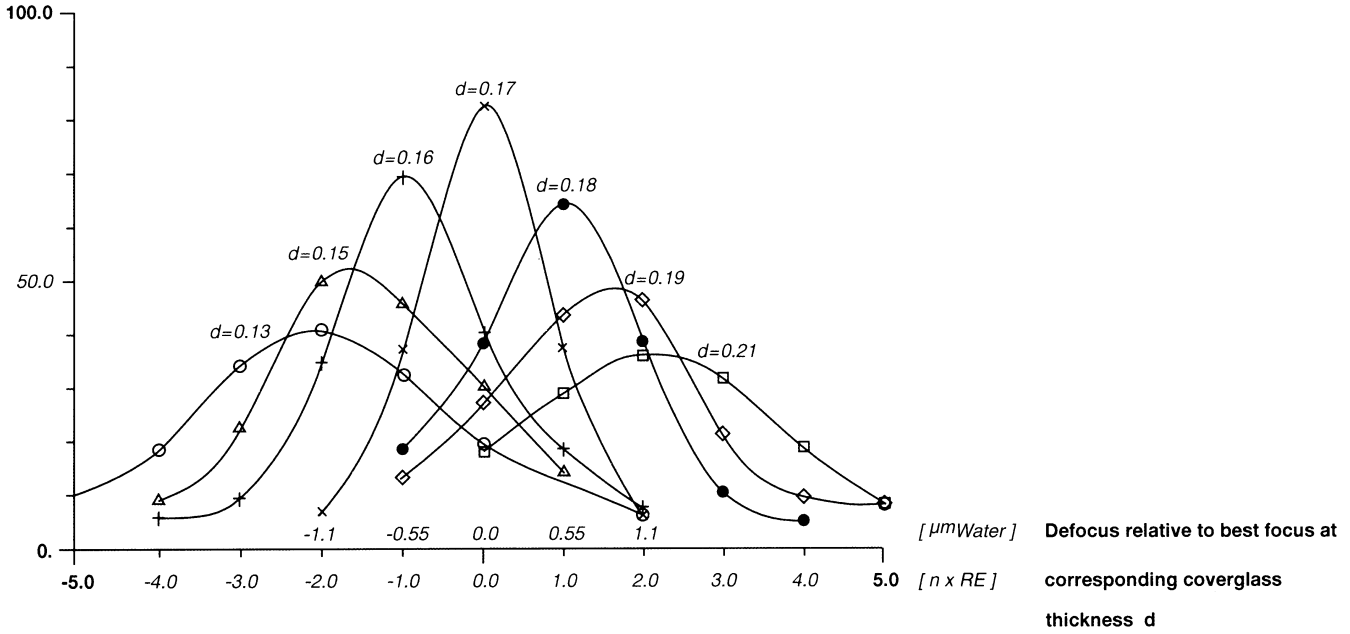


FIGURE 7.10. Pinhole energy as a function of defocus and coverslip thickness (d). Objective 40 \times , NA 1.2 water.

Pinhole energy
 in pinhole $\emptyset = \emptyset$ Airy (543nm, NA=1.3)
 = 20 μm

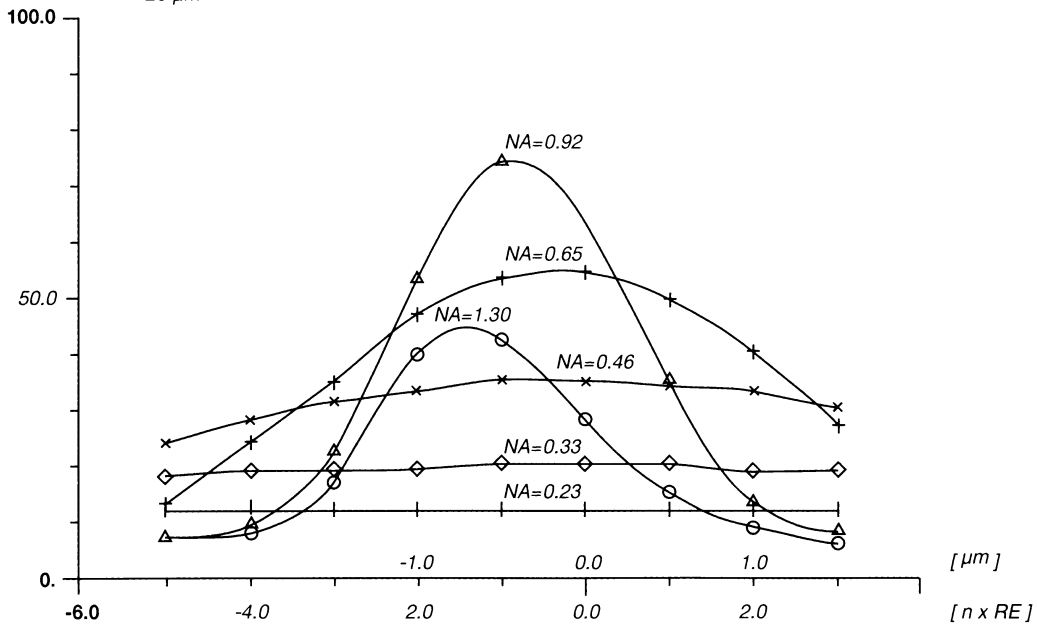
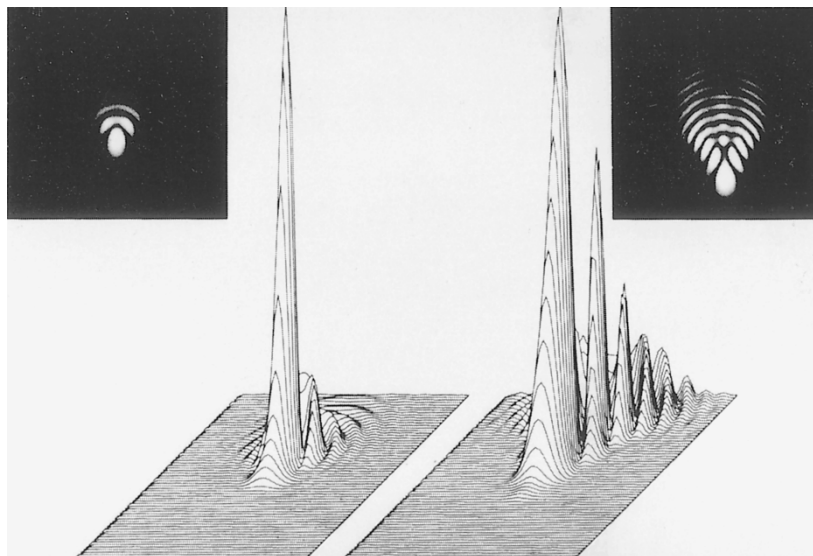


FIGURE 7.11. Pinhole energy as a function of defocus and NA: 40 \times , NA 1.3 objective with iris (variable aperture) penetrating 10 μm into water.

FIGURE 7.12. Intensity distribution in unit image with coma present: slight (left); serious (right).



detected pinhole energy as a function of focus change and NA for a 40× oil-immersion objective with variable NA. At the full NA of 1.3, penetrating 10 μm into a watery medium reduces pinhole energy to <50%, while reducing the NA to 0.92 actually puts more light through the pinhole if one compensates for the reduction in throughput by the lower aperture by increased light input. By reducing the effect of spherical aberration, a larger fraction of the energy reaches the pinhole. However, for $NA \leq 0.5$, the Airy disk becomes significantly larger than the pinhole and the detected energy drops again (see Fig. 7.11). Here we also need to mention a very useful device, called InFocus, from Infinity PhotoOptical (Boulder, CO), which, by varying the effective tube length in a way that does not change the magnification, permits external compensation of spherical aberration to some degree. The system mounts between camera port and the camera (or confocal scan head) and can be motor driven by a computer that also moves the stage to compensate for the small focus changes that occur when the corrector is adjusted (“SAC,” Intelligent Imaging Innovations, Denver, CO).

Coma

For object points away from the optical axis coma, a streaking, radial distortion of the image point is generated (Fig. 7.12). Fulfilling Abbe’s sine condition,

$$r' \eta' \sin \beta' = r \eta \sin \beta$$

where r is the distance from the optical axis; η is the refractive index; and β is the viewing angle, all in image space (') or object space (respectively), eliminates coma and produces an aplanatic system. Unfortunately, all factors with the potential to increase spherical aberration are also especially critical to coma.

As coma is only evident off-axis, it is not important in stage-scanning confocal microscopes. However, it can be important in beam-scanning systems, or when one scans off-axis (even at high zoom) to avoid on-axis specular reflections sometimes visible in the BSL mode.

Astigmatism

For off-axis points, two orthogonal cross-sections through the imaging wavefront (tangential and sagittal) can have different focal distances or radii. When this is the case and a perfectly symmetrical image point in the center of the field is moved off-axis, it

becomes either radially or tangentially elongated, depending on the focus. The intensity ratio of the unit image will diminish, and definition, detail, and contrast are lost with increasing distance from the center.

Figure 7.13 shows the intensity distribution through one section of an astigmatic image point. A four-lobed Airy disk results when the focus is set at the compromise position between the radial and tangential extremes [Fig. 7.13(B)].

Poor lens centration in the objective or poor alignment between the objective, the intermediate optics, and the eyepiece increases both astigmatism and coma. Wedge-error in poor quality filters or dichroics can have the same effect.

Flatness of Field

A simple lens focuses image points from an extended flat object onto a spherical surface shaped like a shallow bowl or dish. Central and peripheral zones are not simultaneously in sharp focus. Prior to the advent of flat-field objectives by Zeiss in the late 1930s, the “usable” field at the intermediate image plane was only 10 to 12 mm. With present-day flat field or “Plan” objectives, ocular fields of 18, 20, and 25 mm exhibit sharp detail from center to edge; however, this improvement has been obtained at the expense of increases in complexity and cost and reduced transmission. In fact, it became practical only after the introduction of anti-reflection coatings.

In Figure 7.14, the field curvature for an achromat and a plan-apochromat are compared. Also shown is the astigmatism of the two orthogonal image spheres. Δ represents the depth-of-field unit

$$\Delta = \frac{\lambda}{\eta(\sin \alpha)^2}$$

It needs to be mentioned here that the term Plan or “F” for flat field is no guarantee for a perfectly flat image with no astigmatism. No standards have been established. Also, the flatness in the final image may be affected by the correction of the eyepiece or other intermediate optics. The diameter of the field of view¹ over which all aberrations have been corrected and the field is flat is listed for a number of Zeiss objectives in Table 7.1.

¹ In the intermediate image plane.

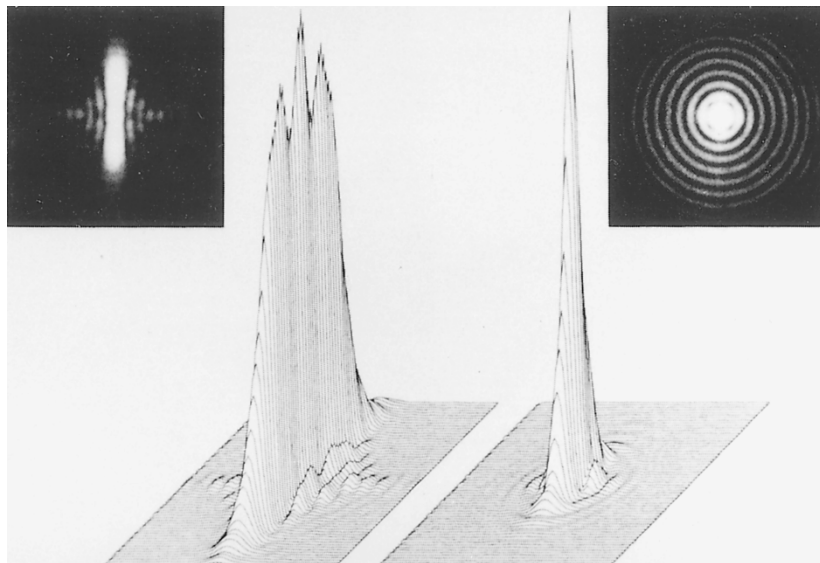


FIGURE 7.13. Intensity distribution in unit image with astigmatism: serious (left); slight (right).

In confocal scanning through thick materials, the dish-shaped section obtained with a non-plan objective may be of little consequence to the biologist, as long as there is no astigmatism or coma and one remains mindful of the distortion this aberration produces in 3D data sets. This is because the exact shape of most biological specimens is often more likely to be distorted by specimen preparation procedures than by optical problems, especially because, when the normal 512×512 image is scanned at Nyquist Zoom magnification, it usually covers only the small part of the field-of-view nearest the axis. The off-axis increase in astigmatism, coma, and field curvature is a good reason to use the “panning” controls, that shift the imaged area away from the optical axis, with caution. However, in materials science and for many critical applications, such as high-resolution imaging in semiconductor inspection, flatness of field is essential.

Distortion

Nonlinear magnification from center-to-edge of field puts the actual, off-axis image point either closer (barrel) or farther away (pincushion) from the axis than the true image point. Barrel or pincushion distortion results, and the true geometry of an object is no

longer maintained in the image. Although less critical in biomedicine than in materials science, distortion is reduced to $<1.5\%$ of the radial distance from the axis in most objectives. It can be checked by imaging crossed grating lines, such as those found in hemocytometers, in the widefield mode. Ideally, the lines should be perfectly straight over the entire image field. A similar specimen can be useful to measure scan linearity in confocal laser-scanning microscopes, however, in this case distortion from nonlinearity of the scan is likely to be larger than that produced by the objective.

Chromatic Aberrations

Wavelength-dependent aberrations are caused by (1) the fact that the η of every optical glass varies with λ , a factor called dispersion; and (2) the fact that λ affects all the dimensions of the unit image point. This latter aberration, called diffraction-caused spreading, is usually barely noticeable in the center of the Airy disk but is more noticeable at the edges of the first fringe, where it influences the resolution. We will discuss this later.

Longitudinal Chromatic Aberration

This aberration is the result of changes in lens focal length, (Δf), with changing λ . In general, the image plane is in sharp focus for only one wavelength or for a narrow wave band. For other wavelengths, the image plane is slightly defocused. Figure 7.15 com-

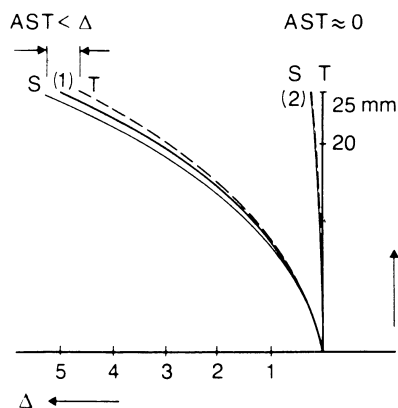


FIGURE 7.14. Flatness of field and astigmatism for (1) achromat and (2) planapochromat as a function of position in the intermediate image plane.

TABLE 7.1. Diameter of Corrected Image for Some Zeiss Plan Objectives

Objective Conventional	Flat Field of View	
	Conventional	Confocal
Planapo 40×/1.2 water corr.	25	12
Achroplan 20×/0.5 water	24	25
Achroplan 100×/1.0 water	18	10

With best focus on the center, the “image disk” will not exceed the depth of field within the specified field; diameter in millimeters.

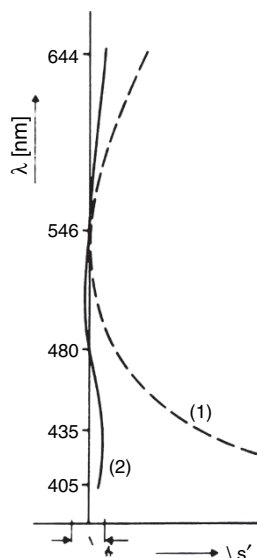


FIGURE 7.15. Longitudinal chromatic correction of (1) achromat and (2) apochromat.

compares the longitudinal chromatic correction of an achromat with that of an apochromat. In order to judge the influence of Δf on the image quality for a given lens, the spectral emission of the source as well as the spectral sensitivity of the detector need to be considered because both determine the effective brightness in the center of the disk (i.e., the energy that passes through the pinhole).

The peak sensitivity for the eye is at 550 nm, with a spectral range of ~ 400 to ~ 650 nm. Figure 7.16 shows the spectral emission of a typical light source and the spectral sensitivity of the eye. If we normalize the response at 550 nm to 100%, the sensitivity of the eye to an image of a sample illuminated by tungsten light is $\sim 10\%$ at 480 nm and $\sim 30\%$ at 640 nm. In confocal scanning, the emission spectrum of the source and the spectral sensitivity of the detector need to be considered along with the emission peak and bandwidth of the specific fluorophore.

Chromatic aberrations are both produced and corrected by utilizing the different dispersions of the glasses used. Glasses of “normal” dispersion have an almost linear decrease in η with

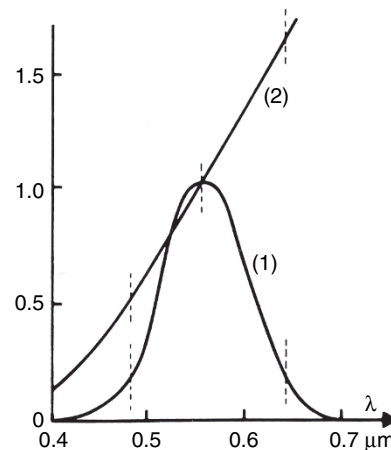


FIGURE 7.16. (1) Spectral sensitivity of the eye. (2) Spectral emission of a tungsten source.

increasing λ and are used for achromats. Only two wavelengths have the same focus, and the remaining “secondary spectrum” produces greenish or purple fringes on images of sharp edges.

For objectives with better chromatic correction, glasses of “abnormal” partial dispersion are needed. Here the refractive index changes more rapidly with wavelength in either the blue or red region.

Abbe used the crystal fluorite (CaF_2) to reduce the secondary spectrum, and more recently, glasses have become available with similar dispersion properties. By replacing any single lens with a doublet containing both a positive and a negative element, with each element having a different dispersion, it is possible to make the chromatic effects cancel out at two or more wavelengths. This has resulted in the high degree of chromatic correction for an apochromat (Fig. 7.15), where up to four or more wavelengths can have the same image location [see Fig. 15(A)].

With apochromat and semiapochromat or fluorite lenses, the “diffraction-caused spreading” of the intensity distribution, referred to above, can also be virtually eliminated, as Figure 7.17 illustrates. An achromat still has substantial intensity in the first fringe, while the apochromat approaches the theoretical resolution

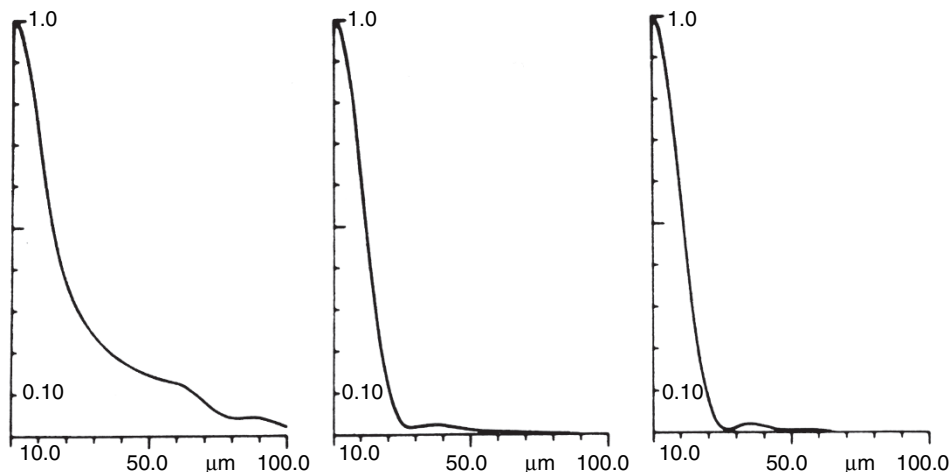


FIGURE 7.17. Intensity distribution in the image of a point object illuminated with white light for an achromat, plan-neofluar, and planapochromat.

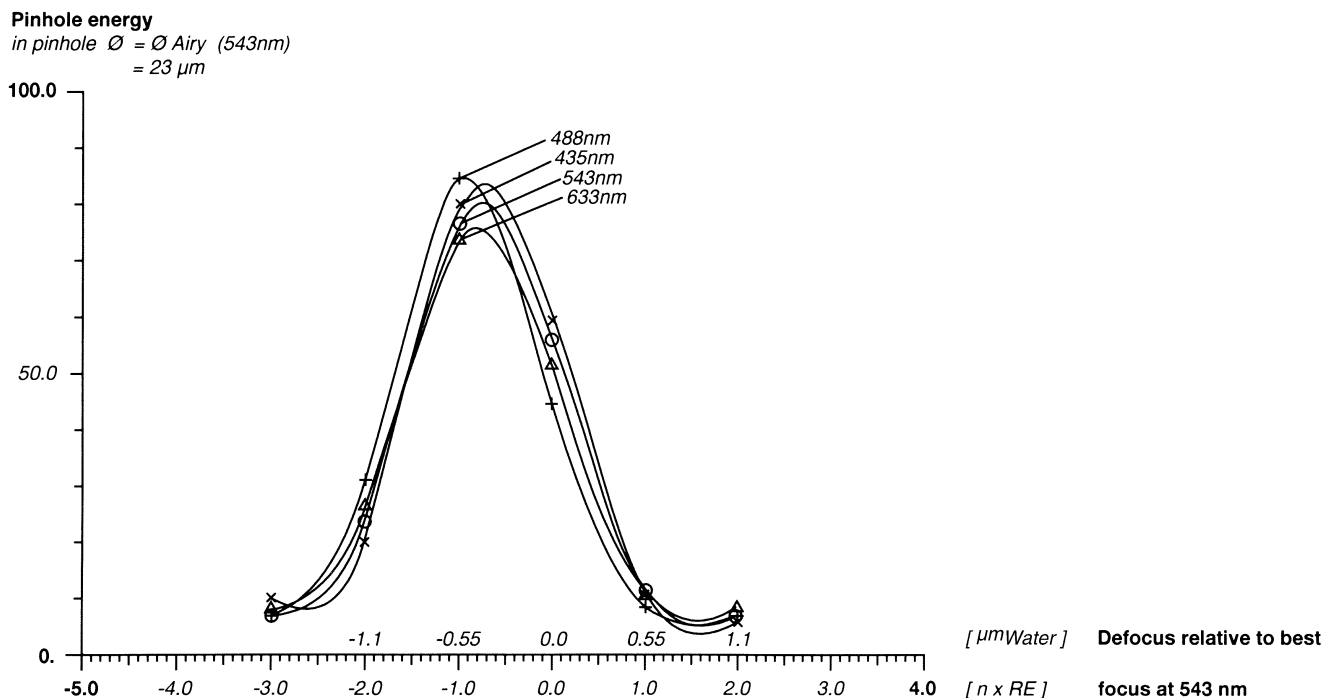


FIGURE 7.18. Pinhole energy as a function of defocus and wavelength: planapochromat 40 \times , NA 1.2 water, $d = 0.17$.

limit where the longitudinal chromatic aberration is $\leq \lambda(\text{NA})^2$, the wave-optical depth of field.

Because the apochromat requires elements of abnormal dispersion, their characteristics may not be ideal for some specific applications, such as fluorescence excitation in the near ultraviolet (UV) or polarizing microscopy. For this reason, a fluorite objective is often more suitable, and Figure 7.17 illustrates how close it comes to the performance of the apochromat.

For confocal scanning fluorescence images, it is important that the correction be as similar as possible at the excitation and emission wavelengths in order to produce the best results in terms of the signal transmission and resolution.

In UV-excited confocal fluorescence with emission in the visible range of the spectrum (e.g., 351 nm and 514 nm), even normal planapochromats will fail to assure precise parfocality. This will result in energy loss at the pinhole unless either one of the new “blue” objectives are employed² or the UV laser is specially adapted with its own optical interface to compensate for the objective’s shortcomings. To accomplish the latter, the beam expander of the UV laser is adjusted to precisely parfocalize the excitation spot in the specimen with the image of the detection pinhole.

Some of the new water-immersion objectives designed for confocal imaging also specifically address the problem of UV excitation, not only by having a high degree of UV transmission, but also by extending the corrected waveband far enough to assure good confocality between UV-exciting and visible-emitted radia-

tion. Specifically for near UV excitation, Nikon offers a CF Fluor 40 \times , NA 1.2 water lens with high transmission down to 340 nm and a working distance of 220 μm . Olympus now offers four UV-apochromats: 20 \times , NA 0.4; 40 \times , NA 0.9; 100 \times , NA 1.1 with working distances of 150 μm , 130 μm , and 130 μm , respectively. All are apochromatically corrected from 350 nm to 600 nm with excellent flatness over a 10 mm field. The Zeiss C-Apochromats 40 \times /1.2 water and 63 \times /1.2 water combine high, near-UV transmission with apochromatic color correction, flatness over a 14 mm field, and working distances of 0.24 mm. Figure 7.18 shows the pinhole energy as a function of focus and wavelength for such an objective.

An interesting and imaginative use for longitudinal chromatic aberration was described by Maly and Boyde (1994) as a means of implementing real-time, stereoscopic confocal microscopy (Boyde and Jones, 1995). They have developed special objectives with linear longitudinal chromatic dispersion (LLCD). When these lenses are used to detect the reflected light signal from a disk-scanning confocal microscope using “white” light illumination, discrete “strata” of the specimen surface appear in only those colors for which confocal conditions exist (i.e., different strata have different colors with the blue layer being closest to the objective and the red layer farthest). These spectral colors can then be either recorded with a color image sensor and converted directly into height by simple computer algorithms or used as the basis of a real-time stereoscopic imaging system. In the latter case, dispersive viewing elements (prisms) are used to change the different colors into a parallax shift that depends directly on the color and indirectly on the height. By mounting two such elements into the two sides of a binocular viewing head so that they have opposite horizontal dispersions, the viewer will perceive a striking, real-time stereoscopic confocal image. The special LLCD objectives described range from 10 \times /NA 0.3 to 120 \times /NA 1.0 (oil).

²These “blue” objectives have been designed to perform best in the near-UV blue end of the spectrum. Other manufacturers also now offer objectives optimized for best performance at near-IR-red wavelengths for using in multiphoton excitation microscopy.

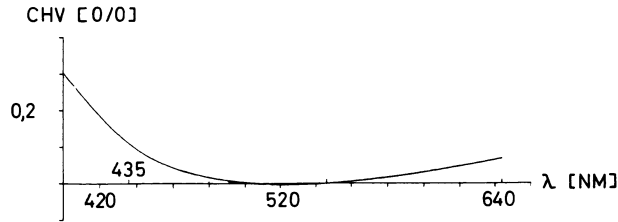


FIGURE 7.19. Lateral chromatic aberration for a Planapo 40 \times , NA 1.2 water.

Lateral Chromatic Aberration or Chromatic Magnification Difference

Because magnification is proportional to $1/f$, the same change of f with λ that causes light of different λ to focus on different planes (producing axial chromatic aberration) also causes the magnification to change with λ , producing lateral chromatic aberration (LCA). If the magnification of an objective is different for different λ , images of sharp edges in the object will show blue or red fringes. In a non-corrected system, the blue component at 436 nm may be imaged 1.4% larger than the red component at 630 nm. Normally, the LCA is greater for objectives of short focal length and the magnification error can range from 1.1% to 1.9% of the radial distance from the optical axis.

In confocal scanning fluorescence, LCA can cause the excited light to return to a location nearer to, or farther from, the axis than the apparent location of the source (see Fig. 35.14, *this volume*). This results in intensity loss at the pinhole. Proper matching of all components is essential to assure full compensation of the LCA. In multi-channel fluorescence, poor registration of blue-, green-, and red-emitting markers can lead to possible errors in mapping their precise locations. A highly corrected lens such as the planapochromat 40 \times , NA 1.2W keeps the LCA well within 0.2% over a wide wavelength range (Fig. 7.19).

In earlier, conventional microscope systems, all objectives were calculated to produce a constant amount of LCA, which was then compensated for by the eyepiece. This compensating system is illustrated in Figure 7.20. The modern, infinity-corrected microscope objectives are either fully LCA-corrected in the objective itself (Nikon, Olympus) or use a compensating tube lens for a full correction of the intermediate image.

The Zeiss ICS (Infinity Color-corrected System) optics are unusual among these tube-lens systems in that no correction for LCA takes place in the objective. The ICS tube lens is a single, spherical lens which fully compensates for LCA (range \cong 1.1%–1.9%) in all objectives over the entire 25 mm intermediate image field (Fig. 7.21). This is possible because, although all off-axis imaging bundles pass through the exit pupil, the position of the exit pupil itself depends on the focal length of the objective (i.e., the magnification): the shorter the focal length, the closer the exit pupil is to the specimen. If we trace off-axis bundles from a short focal length objective to the tube lens, we find that they reach more peripheral zones of the tube lens, which compensate more strongly for the higher LCA present in high-magnification lenses. On the other hand, bundles from long focal-length objectives reach only the more axial zones that are appropriate for the lower LCA compensation needed in low-magnification objectives. Relieving the objective from LCA correction in this way means fewer elements in the objective and a choice of more suitable glass types, particularly for the Plan-Neofluars, where only one selected heavy flint glass and no fluorite is used. This virtually eliminates autofluorescence in the objective, improves extinction ratios for

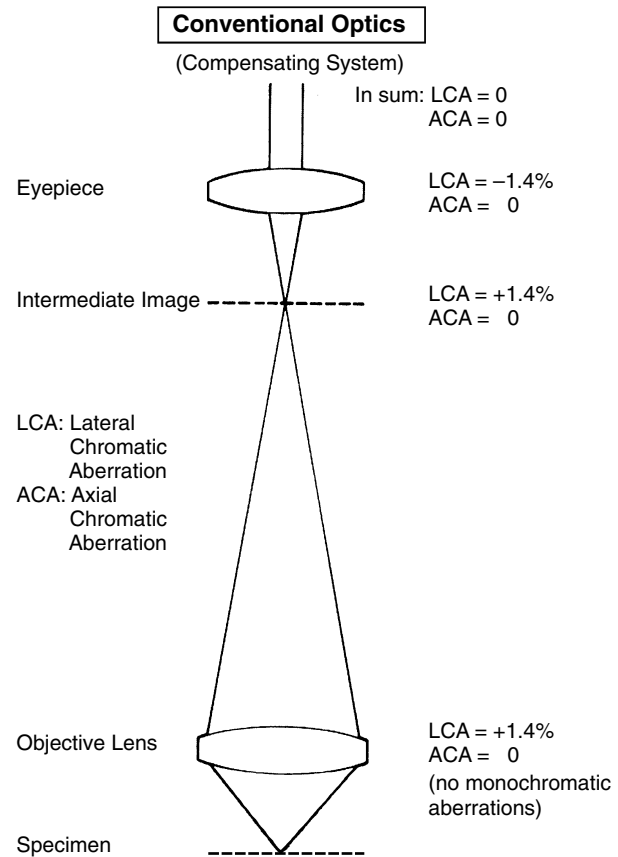


FIGURE 7.20. Correction of lateral chromatic aberration in conventional optics.

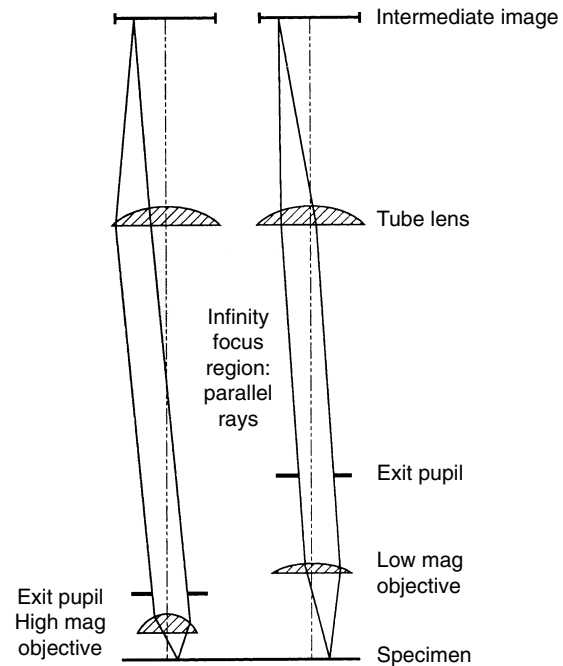


FIGURE 7.21. Zeiss's ICS optics operation. The same tube lens produces more chromatic correction for high magnification objectives than for low magnification objectives because the relative size and position of the exit pupils, and the optics of the infinity-focus objectives themselves, causes rays to pass through different parts of the tube lens (see text for more detail).

polarizing microscopy, and assures high light throughput and good contrast.

All off-axis aberrations can adversely affect the performance of beam-scanning systems. Potentially most critical is LCA in the confocal fluorescence mode, where the excited off-axis object point may be sufficiently shifted from the pinhole that a substantial signal loss may occur.

Example: A 100× oil objective may scan a 100 × 100 μm field in the object with 500 pixels per scan line. Assume that the position of a 0.2 μm diameter blue Airy disk of exciting light is shifted 1.9% of the distance from the center of the field compared to its corresponding red emission disk. Pixels that are 50 μm from the center will be displaced almost 1 μm or 5 pixel diameters away from the pinhole. Depending on the size of the pinhole, the severe loss of signal is obvious.

For confocal microscopy, the LCA — transferred to the specimen field — must be smaller than the pixel spacing on the periphery of the scanned field. For a raster scan of 512 × 512, this means an LCA of less than 0.19%, if we assume the ~1.4× resolution increase of confocal scanning. The LCA for a Planapo 40×, NA 1.2W is shown in Figure 7.19. In more general terms, it means that Nikon CF objectives cannot be replaced by compensating objectives unless the rest of the system optics are also changed.

With the increasing interest in two-photon excitation, which requires optimal chromatic correction for the incoming infrared (IR) beam combined with efficient collection of the emitted photons, more and more lenses for that application have become available.

Reflecting Objectives

At first sight it might appear that a logical solution to the problem of chromatic aberration might be to use reflecting rather than refracting objectives. Reflection is insensitive to λ and, like the reflecting telescope, a reflecting microscope objective could offer excellent chromatic correction over a wide spectral range. In fact, some low and medium power reflecting objectives are routinely used particularly for far-IR microscopy. However, high resolution requires objectives with high NA and short focal length or even immersion systems. Though the diamond-turning lathe could produce the aspherical surfaces required with the necessary precision, such lenses cannot now be produced at reasonable cost. Furthermore, an inherent limitation of reflecting objectives is the elimination of paraxial imaging bundles with the corresponding loss of diffraction orders and effective NA.

FINITE VERSUS INFINITY OPTICS

Some conventional microscopes still in use were built around the German DIN (now ISO) standard, which calls for the objective to form a real image at a tube length of 160 mm. The parfocal distance is set at 45 mm and the object-to-image distance is 195 mm (Fig. 7.22). This standard applies to many transmitted light techniques and has served us well for over 50 years.

Objectives with a finite image distance form a real, intermediate image directly. This intermediate image may either be corrected (Nikon) or it may have residual LCA to be compensated for by the eyepiece. Infinity-designed objectives require a tube lens to form this real, intermediate image. While this tube lens can also be employed to correct for residual aberrations, the intrinsic design advantage of infinite image distance (Fig. 7.23) is its relative insensitivity to optical components (such as filters, analyzers, compensators, DIC prisms, and reflectors) in the telescopic space between

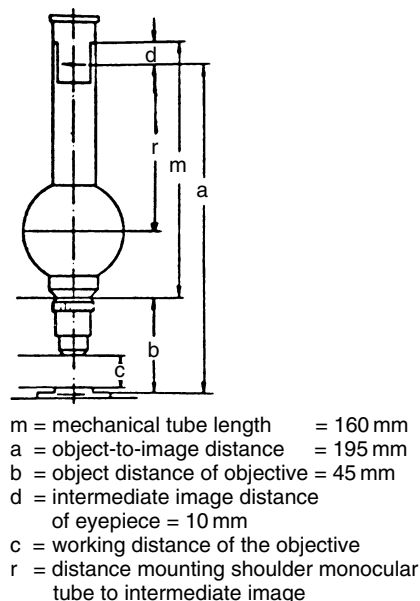


FIGURE 7.22. Standard dimensions of DIN standard conventional microscope.

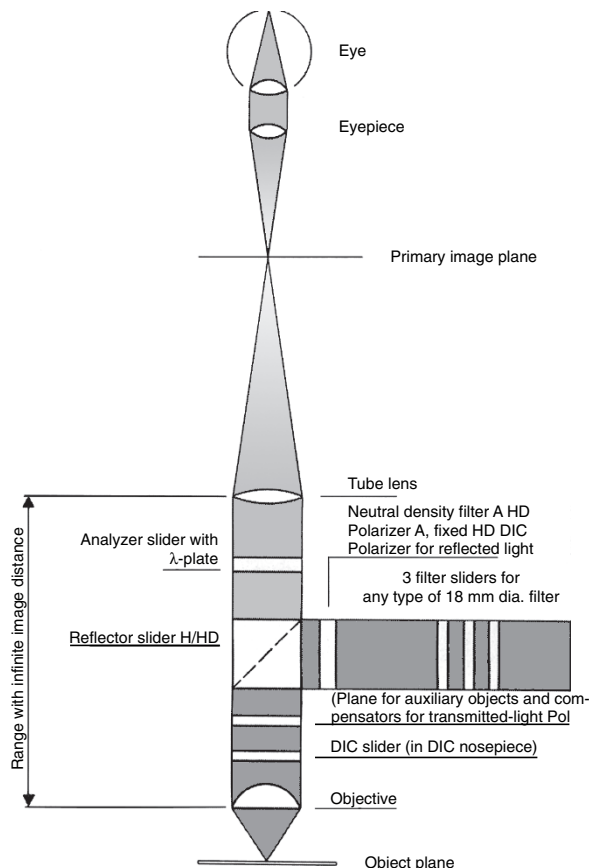


FIGURE 7.23. Advantage of using objectives with infinity correction. A number of accessories, such as the Wollaston prisms used for DIC and the filters for epi-fluorescence, can be introduced between the objective and the tube lens without affecting the image of the structure at the front focal plane.

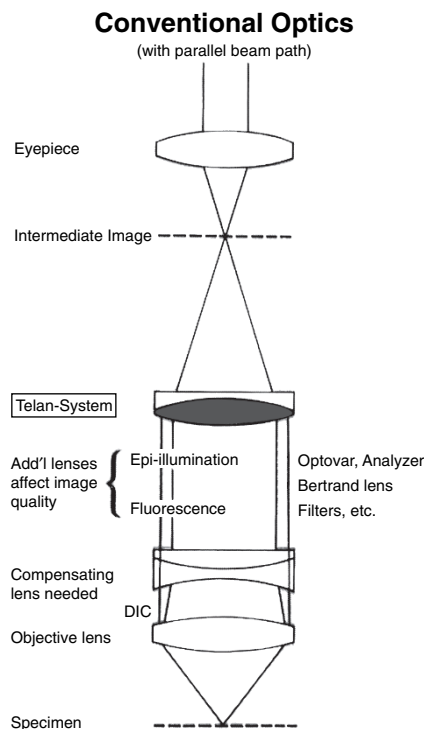


FIGURE 7.24. Conventional optics using Telan lenses. Requires more components that not only reduce resolution and cause reflection losses but also increase magnification.

objective and tube lens. Infinity or parallel beams are not affected by the thickness or η of such components as long as they are plane parallel. The location of the image point remains constant, both axially and laterally, as does the alignment between the objective and the tube lens.

Another advantage of infinity-corrected optics is that one can focus by moving the objective rather than having to move the stage, as is the case in most inverted and some upright microscopes.

In the converging beam path behind a 160 mm tube length objective, similar elements would cause axial, and possibly lateral, shift. This not only causes aberrations but makes it difficult to get good image registration in multi-parameter techniques (double or triple fluorescence). To avoid this, so-called Telan systems are added to generate an “infinity space” into which the “flat” components can be introduced. This eliminates the image shift and dis-

ortion but only at the cost of two additional optical elements — one negative and one positive — and with them some additional magnification (usually 1.25 \times) and the potential for more flare and stray light (Fig. 7.24).

The design concepts followed by major microscope manufacturers are summarized in Table 7.2.

WORKING DISTANCE

For reflected light objectives, the distance between the focus plane and the closest structural element of the objective is called the working distance (WD). For transmitted light lenses, the specified free working distance is the distance from the coverslip to the closest structural element of the lens. In a confocal microscope, the WD sets an absolute limit that the focus plane can be below the top surface of the coverslip. As an optical design parameter, WD can be varied over a considerable range, but, as can be seen from Table 7.3, it becomes decidedly shorter in objectives with higher NA and greater correction.

In oil lenses, the first refracting surface struck by a light ray is the far side of the first element of the objective. This surface is often a segment of a sphere that is large enough to encompass the full NA of the design. (The lens half-angle, α , is 74° at NA 1.4.) As the focus plane moves away from the glass, this sphere segment must become larger with the result that soon there is no longer sufficient space in which to install the other elements needed for chromatic and field corrections. These larger elements are also more expensive to produce.

When working with living materials, the matter of WD can have a second aspect because in such cases, it is often convenient to be able to change the z -position of the imaged plane in the object without actually moving either the position of the front surface of the objective or the specimen itself. This can occur when imaging the living eye where actual contact between the cornea and the objective is needed to reduce the effect of pulse-induced motion. To solve this problem, Petroll and colleagues (1993) have used an objective with internal focusing elements to permit changes in focus plane while maintaining mechanical contact.

The working distance is a critical issue for 3D imaging of thick samples or when manipulation or probing under the objective is required. However, we must also keep in mind that thick layers of medium between object and objective can easily create turbulence (e.g., when focusing) or inhomogeneities (such as air bubbles!) that can seriously impair image quality or signal intensity.

TABLE 7.2. Tube Length and Chromatic Corrections of the Major Microscope Manufacturers

Manufacturer	Mode	Fixed, Finite Tube		Chromatic Correction
		Length (mm)	Length (mm)	
Leica	Reflected	—	200	In-tube lens
	Transmit (older)	—	200	In-tube lens
		160	—	Leica correction
Nikon	Reflected (few) (most)	—	210	None required
		210	—	None required
	Transmit	160	—	None required
Olympus	Reflected	—	180	In-tube lens
	Transmit (some) (older)	—	180	In-tube lens
		160	—	Olympus correction
Zeiss	Reflected	—	160	Universal tube lens
		—	160	Universal tube lens
	Transmit (older)	160	—	Zeiss correction

TABLE 7.3. Working Distance of Some Zeiss Objectives

Objective	Immersion	Cover Glass	Working Distance
Epiplan 50×/0.5	Air	No	7 mm
Epiplan 100×/0.75	Air	No	0.98 mm
Epiplan-Neofluar 100×/0.9	Air	No (correction collar)	0.28–0.31 mm
LD Plan-Neofluar 40×/0.6	W/Gly	Yes (correction collar)	2.5–3.3 mm
Planapo 40×/0.95	Air	0.13–0.17 (Correction collar)	0.16 mm
Achroplan 40×/0.8	Water/dip	No	3.61 mm
Achroplan IR 63×/0.9	Water/dip	No	2.2 mm
Achroplan 100×/1.0	Water/dip	No	1.00 mm
c-Planapo 40×/1.2	Water	Yes	0.22 mm
Planapo 100×/1.4	Oil	Yes	0.17 mm

OPTICAL MATERIALS

More than 200 optical glasses are available to the optical designer. Their properties, such as refractive index, dispersion, transmission, contaminants, potential for auto-fluorescence, chemical and thermal resistance, and overall homogeneity are usually carefully selected to ensure superb optical performance. However, this may compromise other requirements, such as high transmission in the near-UV range or high extinction factors in polarizing microscopy. Some new materials, such as fluorocrown glass, approach the properties of natural fluorite while avoiding most of its drawbacks, such as the presence of organic contaminants and a crystalline structure that can seriously degrade performance in fluorescence and polarizing microscopy. Fully apochromatic correction, however, still requires both natural fluorite and glasses that have low transmission in near UV.

Therefore, the semi-apochromat is often the ideal compromise. It can be a true multi-purpose objective, combining excellent correction with good contrast, high NA, and high spectral throughput.

Even though their thickness is usually $<10\mu\text{m}$, the cements between doublet or multiple lens elements can have spectral absorption properties that may render an objective unusable for specific applications.

The chemical and optical properties of optical glasses are usually proprietary. Decementation between lenses, caused by heat and different coefficients of expansion, is rare. Lasers of $<100\text{mW}$ energy in near-UV and visible range will cause no damage if their power is evenly distributed over the entire entrance pupil, however, damage can occur if a similar amount of light is brought to a focus on any optical surface having an appreciable absorption at that λ .

ANTI-REFLECTION COATINGS

As the sophistication of objectives increases, more elements are required, and this accentuates the need to eliminate internal reflections to produce higher transmission, better contrast, and less flare, particularly in incident- or reflected-light applications. Single-layer anti-reflection (AR) coatings dating back to the 1940s have since been refined and supplemented by multi-layer coatings, increasing the transmission in the visible spectral range through an air-glass interface from $\sim 96\%$ (not coated) to $\sim 99\%$ (single layer coating) to $\sim 99.9\%$ (multi-layer coating) (Figs. 7.25 and 7.26).

Coating materials can be magnesium fluoride and a multitude of proprietary materials (see Chapter 3, *this volume*), all of which have their own optical properties potentially affecting the trans-

mission of the system in given spectral regions. In general, the interference characteristics of AR coatings are spectrally limited, and constructive interference for high transmission in the visible range means destructive interference in harmonically related frequencies outside the transmission band.

For specimens of very low reflectivity, the weak BSL signal may be overwhelmed by background light produced by internal reflections in the objective lens or other optical surfaces that reflect light that comes to a focus near an image plane. In this case, a so-called Antiflex system can have a great advantage. In this approach, we illuminate with polarized light and observe through an analyzer at 90° to the polarizer (Chapter 10, *this volume*). Because stray light produced by specular reflection from optical surfaces retains its direction of polarization, it can be blocked by the analyzer. If a $1/4$ wave plate is incorporated into the front element of the objective with its vibration direction diagonal to both the polarizer and analyzer for a specific wavelength (usually 550nm), this will generate circularly polarized light below the objective. The $1/4$ wave plate rotates the plane of vibration of both the illumination and the returning BSL by 45° for a total of 90° , so light reflected from the object is now oriented parallel to the analyzer and can pass freely to the detector. This system is used for the so-called reflection contrast or reflection interference techniques but is also most effective in confocal studies of weakly scattering objects (Pawley *et al.*, 1993).

Transmission of Microscope Objectives

We have seen that a number of factors influence the spectral throughput of an objective: glasses, cements, coatings. However, these considerations must apply to not only the objective but to the whole system if it is to provide high transmission in the desired wavelength range.

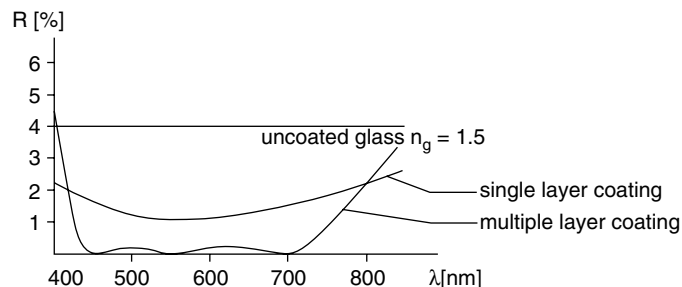


FIGURE 7.25. Reflectivity of glass surfaces covered with single- versus multi-layer coatings.

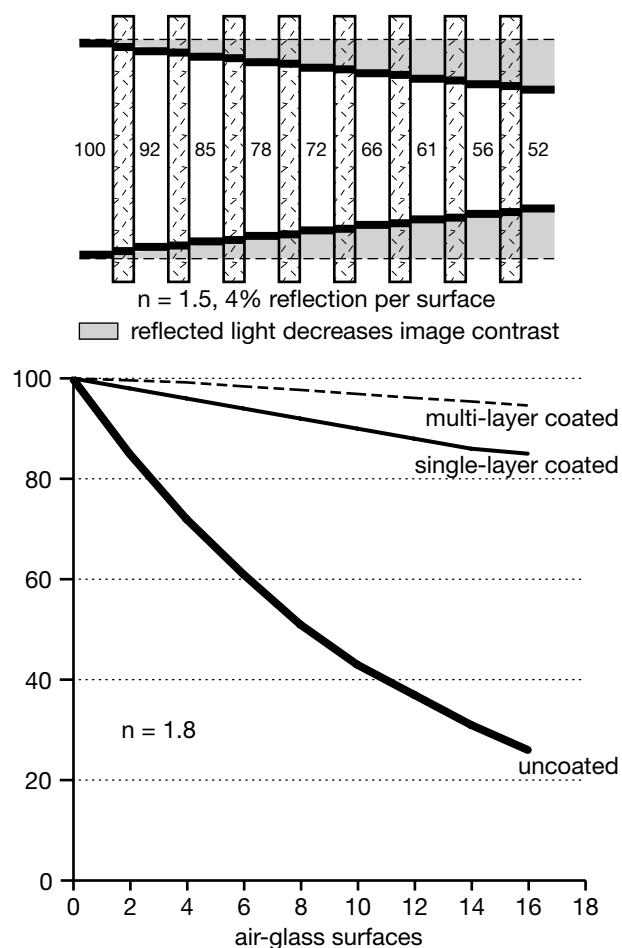


FIGURE 7.26. Reflections on surfaces of $n = 1.5$ (above) versus $n = 1.8$ (below). At $n = 1.5$, the eight elements with their 16 surfaces, each reflecting 4%, result in a throughput of only 52%. At $n = 1.8$, the 16 uncoated surfaces would pass only 26%. Single-layer anti-reflection coating increases total transmission to 85%, and multi-layer coating to 94.6%. This increase in throughput, and corresponding reduction in internal scatter and “noise,” substantially enhances the contrast of the image because it both makes bright features brighter and dark features darker.

A typical arrangement to measure the spectral transmission of an objective is shown in Figure 7.27: light source (tungsten halogen and/or xenon) with monochromator and iris diaphragm fill the objective’s back-aperture. A parallel light beam equal in diameter to the pupil of the objective strikes the rear of the objective and emerges through the front lens where it is collected by an integrating sphere and measured by a PMT with photometer read-out. The result is compared to a second measurement made with the objective removed.³

Table 7.4 shows the relative spectral transmission of several representative objectives that have been optimized for high transmission in the near-UV. With confocal fluorescence microscopy extending both towards the near UV as well as towards the IR, the

³The high-NA rays from an oil-immersion objective can only escape from the glass into the sphere if a small, planoconvex lens is attached to the front element with oil.

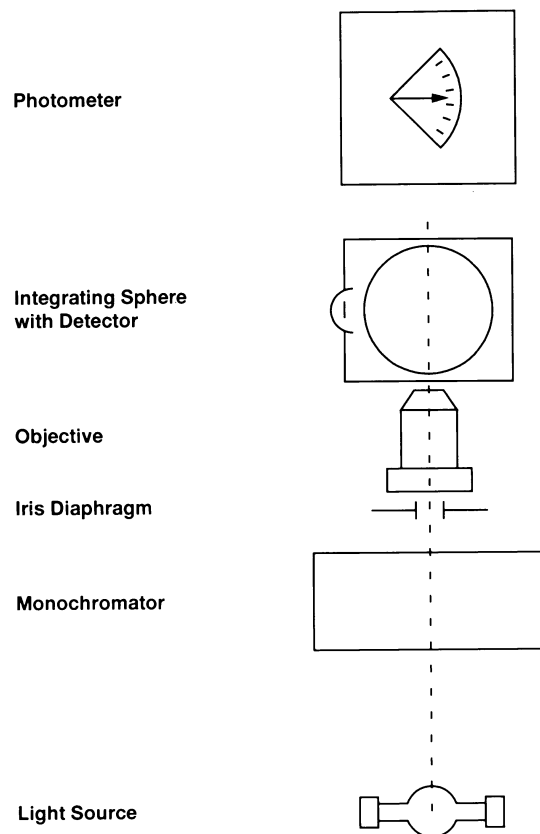


FIGURE 7.27. Setup to measure an objective’s spectral transmission.

spectral transmission of a total system needs to be looked at. The transmission curves for a number of objectives by Nikon, Leica, and Olympus are included in the Appendix at the end of this chapter. Keep in mind that these transmission curves are typical only for a given lens. Tolerances, particularly in the AR coating, can introduce significant variations, particularly at the cut-on and cut-off ends of the transmission curve.

Depending on the application, objectives can be chosen with high throughput in the near-UV or with extended IR transmission. Having good transmission in both the near-UV and the near-IR is not possible.

A number of new objectives, designed specifically for confocal microscopy, are either already available or in preparation. More detailed information on their performance and spectral throughput is best obtained directly from the manufacturers.

TABLE 7.4. Relative Transmission of Some Typical Objectives

Manufacturer	Objective	Wavelength (nm)				
		320	350	400	500	600
Nikon	Fluor 40×/1.3 oil	16%	66%	80%	90%	91%
Olympus	UVSLM 40×/0.9 water	—	56%	—	88%	—
	UVSLM 100×/1.1 water	—	60%	—	90%	—
Zeiss	Fluor 40×/1.3 oil	29%	79%	88%	95%	99%
	Planapo 40×/1.2 water	20%	54%	86%	89%	92%
	Achropam 100×/1.0 water	—	605	90%	94%	90%

CONCLUSION

Many modern microscope objectives are well suited for confocal scanning as long as they are used within their design specifications. With the ever-wider use of confocal scanning microscopy for 3D live-cell imaging and with new microscope techniques emerging, new and improved objectives continue to appear. Often they are optimized for a specific application. This trend will continue. Just a few examples are the new highest-NA 60×/1.45 and 100×/1.45 oil-immersion lenses or the special objectives Olympus introduced for epi-illuminated total internal reflection fluorescence (TIRF) microscopy with an NA of 1.45 or 1.65. It follows from the discussion above that the latter NA requires a special immersion medium and rather costly high-index coverglasses.

In addition to the call for objectives with higher NAs, longer working distances, and maximum transmission in the visible and UV, this may be the place to “dream” about other exotic lens features. We might imagine a tunable objective, a lens whose chromatic correction can be “tuned” to the specific excitation and emission wavelengths actually in use to produce the best image quality with only a few elements and high transmission. If such tunability is impossible, perhaps special achromatic lenses will be designed for use with specific fluorophore/laser combinations, such as the “blue” objectives recently offered by Leica.

An even more exotic dream (included in the second edition of this volume) for a substantial increase in signal intensity realized by using two, matched lenses above and below the specimen, has now been commercially realized in the Leica 4Pi microscope (Chapter 30, *this volume*). On optically homogeneous specimens, equipping the “far” objective with a reflector to return the spot into itself, might not only increase photon efficiency but also might permit combining reflected and transmitted confocal scanning.

As mentioned earlier, two-photon excitation, will probably also spawn the development of special objectives, not only in terms of their spectral characteristics but with spherical and chromatic correction optimized for the IR, such as the recent “IR” objectives from Olympus.

For the study of live organisms, one needs water-immersion objectives that combine the long working distance needed for deep

penetration, with the highest possible NA for better resolution and improved photon collection efficiency.

These are just a few thoughts on possible future developments in this area. No doubt, specialists in optical design will quickly return us to reality and make us do with less than our dreams.

ACKNOWLEDGMENTS

Many thanks to a number of scientists at Carl Zeiss, Germany, for their help in preparing this paper and for many of the illustrations. Special thanks to Mr. Franz Muchel, head of the mathematics group at Carl Zeiss, whose paper (Zeiss Information #100, 1/89, 20–27) on ICS optics has been particularly helpful, to Dr. Bernd Faltermeier for much support, and to Willi Ulrich, who provided many of the computer simulations and other valuable suggestions.

REFERENCES

- Inoué, S., and Oldenbourg, R., 1995, Optical instruments: Microscopes, In: *Handbook of Optics* (M. Bass, ed.), 2nd ed., McGraw-Hill, New York, pp. 17.1–17.52.
- Boyde, A., and Jones, S.S., 1995, Mapping and measuring surfaces using reflection confocal microscopy, In: *Handbook of Biological Confocal Microscopy*, 2nd ed., Plenum, New York, pp. 255–266.
- Maly, M., and Boyde, A., 1994, Real-time stereoscopic confocal reflection confocal microscopy using objective lenses with linear longitudinal chromatic dispersion, *Scanning* 16:187–193.
- Pawley, J.B., Amos, W.B., Dixon, A., and Brelje, T.C., 1993, Simultaneous, non-interfering collection of optimal fluorescent and backscattered light signals on the MRC 500/600. In: *Proceedings of the 51st Annual Meeting of the Microscopy Society of America*, San Francisco Press Inc., San Francisco, pp. 156–157.
- Petroll, W.M., Cavanaugh, H.D., and Jester, J.V., 1993, Three dimensional imaging of corneal cells using in vivo confocal microscopy, *J. Microsc.* 170:213–219.
- Shimizu, Y., and Takenaka, H., 1994, *Microscope Objective Design in Advances in Optical and Electron Microscopy* (C. Shepard and T. Mulvey, eds.) Academic Press, San Diego, pp. 249–334.

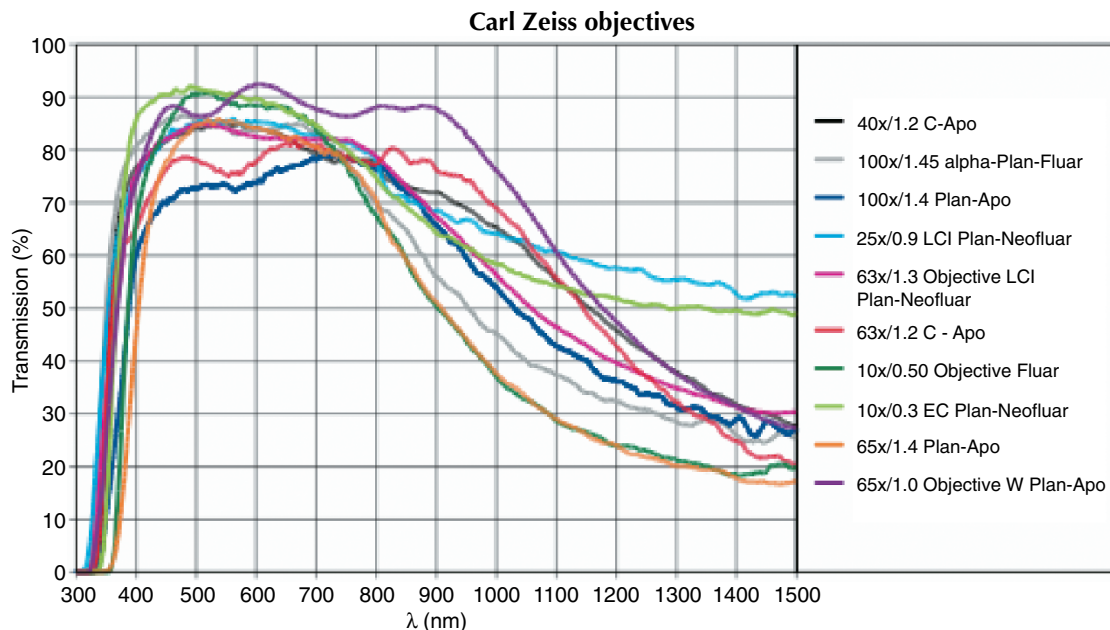
APPENDIX: LIGHT TRANSMISSION SPECIFICATIONS FOR A NUMBER OF MODERN OBJECTIVES MADE BY DIFFERENT MANUFACTURERS.⁴

Leica objectives

Objective	Mag	NA	WD(μ)	T(350)%	T(546)%	T(900)%	Blue	Immersion
HC PL APO 10×/0.40 CS	10	0.40	2200	40	90	75		dry
APO L 20×/0.50 W UVI	20	0.50	3500	60	91	75		water
HC PL APO 20×/0.70, multi-imm, collar	20	0.70	260	40	87	71	•	water/glycerol/oil
HCX PL APO 63×/1.40-0.60 oil	63	1.40	100	20	82	63	•	oil
HCX PL APO 63×/1.30 glycerin collar	63	1.30	280	18	87	64		glycerol : water, 80:20
HCX PL APO 63×/1.2 W Corr	63	1.20	220	16	85	65		water

Blue = Blue variant available with color correction optimized in blue range for UV applications and GFPs with 405 or 430 excitation

⁴ The specifications printed in this chapter are as supplied to the author by the manufacturers at the time that this book went to press (May 2005). The author and the editor have endeavored to insure that the printed versions of these specifications accurately reflect the reports that they received or that were available on the Internet. We make no other claim and readers are advised that improvements are to be expected and will doubtless be announced on the Internet.



Nikon objectives

Objectives	N.A.	Coverglass (mm)	Working Distance (mm)	Trans % @350nm*	Trans % @550nm*	Trans % @900nm*
CFI PLAN ACHROMAT 100× OIL	1.25	0.17	0.20	B	A	A
CFI PLAN APO 20×	0.75	0.17	1.00	E	A	B
CFI PLAN APO 40× w/collar,	0.95	0.17	.12-.16	E	A	B
CFI PLAN APO 60× A OIL IR	1.40	0.17	0.21	E	A	B
CFI PLAN APO 60× WI w/collar	1.20	0.15-0.18	0.22	E	A	B
CFI PLAN APO VC 60× WI	1.20	0.13-0.19	0.27	E	A	B
CFI PLAN FLUOR 20× mult-imm	0.75	0.17	.033-.035	B	A	A
CFI PLAN FLUOR 40×	0.75	0.17	0.72	A	A	A
CFI PLAN FLUOR 100× OIL	1.30	0.17	0.20	B	A	A
CFI SUPER FLUOR 40× w/collar	0.90	0.17	0.30	B	A	B
CFI SUPER FLUOR 40× OIL	1.30	0.17	0.22	B	A	A
CFI W FLUOR 60× dipping	1.00	n/a	2.00	B	A	A
CFI PLAN 100× dipping	1.10	n/a	2.50	E	A	A
CFI Plan Apo TIRF 60×H w/collar	1.45	0.17	0.13	E	A	B
CFI Plan Apo TIRF 100×H	1.45	0.17	0.13	E	A	B

Key: For transmission percentages: A = > 71%, B = 51-70%, C = 31-50%, D = 16-30%.

